

Measurement of bremsstrahlung-induced reaction cross-section for ^{93}Nb using electron Linac

By R. Crasta¹, H. Naik^{2,*}, S. V. Suryanarayana³, S. Ganesh¹, P. M. Prajapati⁴, M. Kumar⁵, T. N. Nathaniel², V. T. Nimje⁵, K. C. Mittal⁵ and A. Goswami¹

¹ Department of Studies in Physics, Microtron Centre, Mangalore University, Mangalagangothri-574 199, Karnataka, India

² Radiochemistry Division, Bhabha Atomic Research Centre, Mumbai-400085, India

³ Nuclear Physics Division, Bhabha Atomic Research Centre, Mumbai-400085, India

⁴ Physics Department, Faculty of Science, The M.S. University of Baroda, Vadodara-390002, India

⁵ Accelerator & Pulse Power Division, Bhabha Atomic Research Centre, Mumbai-400085, India

(Received January 20, 2012; accepted in final form January 28, 2013)

(Published online July 15, 2013)

$^{93}\text{Nb}(\gamma, n)^{92}\text{Nb}$ cross-section / $^{197}\text{Au}(\gamma, n)^{196}\text{Au}$ reaction /
End point bremsstrahlung energy of 10 and 12.5 MeV /
Off-line γ -ray spectrometric technique / TALYS calculation

Summary. Cross sections for (γ, n) reaction at bremsstrahlung end point energies of 10 and 12.5 MeV on niobium have been measured by the activation technique. Induced activities were measured by a high-resolution γ -ray spectrometer with a high-purity germanium (HPGe) detector. Theoretically the (γ, n) cross-section of ^{93}Nb as a function of photon energies were also calculated using TALYS 1.4 computer code. We compared the measured data with the flux weighted average values from the available literature data based on experiments with mono-energetic photons and the theoretical calculation by the model code TALYS 1.4. The experimental values are found to be in good agreement with the theoretical value from TALYS 1.4 but are slightly higher than the flux-weighted values from mono-energetic photons.

1. Introduction

Photo-induced reaction cross section data are of great importance to study the structure of nuclei and mechanisms of nuclear reactions. The cross section induced by photons are useful for various applications – radiation shielding design, calculations of absorbed dose in the human body during radiotherapy, activation analysis, nuclear waste transmutation, astrophysical nucleo-synthesis, physics of fusion and fission reactors [1]. The cross section data by medium-energy photon, proton- and neutron-induced reactions are essential for accelerator driven sub-critical systems (ADSs) to calculate the radioactive inventories of the spallation target, cladding material and structural materials [2–4].

The safety and reliability of a reactor largely depend on the cladding performance. The cladding tube is subjected to various thermal and multiaxial stress conditions inside the reactor [5]. The presence of Nb in Zr-Nb alloys improves the long term corrosion resistance and mechanical

properties [6–8]. This is because niobium has a low thermal-neutron cross section and can be alloyed with zirconium for use in the cladding of nuclear fuel rods, leading to extended fuel cycles with higher burn-ups. Recently, several Nb modified Zr alloys (such as Zirlo) have been developed for use in cladding applications [9]. A Zr-1%Nb alloy has been used as primary cladding in the countries of the former USSR and in Canada. A Zr-2.5 wt. %Nb alloy has been used to replace Zircaloy-2 as the cladding in Candu-PHW reactors.

High power proton accelerators are being developed worldwide for ADS applications. The energy of the proton/deuteron required for this purpose is \sim GeV. Research on Accelerator Driven Systems (ADSs) is being carried out around the world primarily with the objective of waste transmutation. One area of interest is to use ADSs to provide an external neutron source for a sub-critical reactor to transmute long-lived radioactive waste into shorter-lived products [10, 11]. The neutrons are produced by the accelerator beam *via* the spallation process. In ADS, high energy (GeV) protons from the accelerator strike a heavy metal target like W, Pb-Bi, Th and U, ejecting neutrons by spallation reactions. These neutrons then strike other nuclides, which in turn eject other particles. The cascade continues until the energy is spent. In the spallation processes, along with high-energy neutrons, high energy photons are also produced, which can cause fission chain reaction of the spallation target as well as different types of nuclear reaction of the cladding and structural materials of the reactor. Thus, it is important to measure the neutron- and photon-induced reaction cross-section of structural materials such as Fe, Ni, Cr *etc.* as well as cladding material such as Nb.

Previous measurements on (γ, n) reaction on niobium have been performed using mono-energetic photons [12] and from electron bremsstrahlung [13]. However, the available data [12] measured the $^{93}\text{Nb}(\gamma, n)^{92}\text{Nb}$ reaction cross-section using the neutron counting technique. The $^{93}\text{Nb}(\gamma, n)^{92}\text{Nb}$ reaction cross-section are available in Ref. [13] for bremsstrahlung energies above 26 MeV but not at the lower energy side. In a reactor and particularly in ADSs the photons produced stem from bremsstrahlung

*Author for correspondence (E-mail: naikhbarc@yahoo.com).

over a wide range of energies. Thus the bremsstrahlung induced reaction cross-section of Nb is of primary interest for reactor design. In the present work, the $^{93}\text{Nb}(\gamma, n)^{92}\text{Nb}$ reaction cross-sections are determined at bremsstrahlung end point energies of 10 and 12.5 MeV using an activation technique followed by off-line γ -ray spectrometry. The $^{93}\text{Nb}(\gamma, n)^{92}\text{Nb}$ reaction cross-sections induced by 10 and 12.5 MeV bremsstrahlung was also calculated theoretically using the TALYS 1.4 code [14] and the result was compared with experimental value of the present work.

2. Experimental details

The electron linear accelerator of the electron beam centre (EBC) at Kharghar, Navi Mumbai, India was utilized in the present experiment. Two sets of irradiation were done at bremsstrahlung end point energies of 10 and 12.5 MeV to measure the cross-sections of the $^{93}\text{Nb}(\gamma, n)^{92}\text{Nb}$ reaction. In each set a sample stack (Nb-Au) was made. In the first set, the high purity natural niobium and gold metal target foils were weighing about 0.04 g and 0.0525 g, whereas in the second set the weight of niobium and gold were 0.0793 g and 0.1297 g, respectively. All samples were wrapped individually with 0.025 mm thick super pure aluminum foil. The gold foil was used to calibrate the bremsstrahlung flux.

The bremsstrahlung radiation was generated when the pulsed electron beam hit a 0.25 mm thick water cooled tantalum (Ta) target. The 0.25 mm thickness of the Ta foil was chosen in order to avoid the production of neutrons. The tantalum target on a suitable stand is located at a distance of 3 cm from the beam exit window and the samples were kept at a distance of 10 cm from the tantalum target. A schematic diagram of the Nb-Au sample stack for irradiation along with the electron to bremsstrahlung converter is shown in Fig. 1. Each of the target samples were placed below the tantalum foil for individual irradiation. The foils were then irradiated for 4–5 h with the bremsstrahlung radiation with end point energies of 10 and 12.5 MeV. In the first set of experiments, for 10 MeV bremsstrahlung the electron LINAC was operated with a pulse repetition rate (PRR) of 310 Hz, a pulse width of 10 μs and an average beam current of 33 mA. In the 12.5 MeV bremsstrahlung irradiation, the electron LINAC was operated with a PRR of 300 Hz, a pulse width of 10 μs and an average beam current of 25 mA. After the irradiation, the samples were cooled for 2–3 h. Then, the irradiated targets of Nb and Au along with an aluminum catcher were mounted on different Perspex plates and taken for γ -ray counting.

The γ -ray activities emitted from the activated foils were measured by using an energy- and efficiency-calibrated 80 cm³ HPGe detector coupled to a PC based 4K channel analyzer. The resolution of the detector system was 2.0 keV at 1332.0 keV of ^{60}Co . The sample was kept at a suitable distance from the detector to minimize the loss of counts. At the same time the dead time of the detector system was kept below 10% to avoid the coincidence effects. The energy- and efficiency-calibration of the detector system was done by counting the γ -ray energy of a standard ^{152}Eu source. The photo peak areas under the individual gamma rays were determined by analyzing the gamma-ray spectra using the

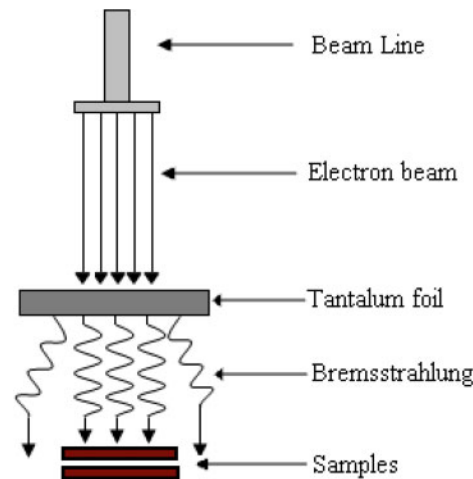


Fig. 1. Schematic diagram showing the arrangement used for bremsstrahlung irradiation.

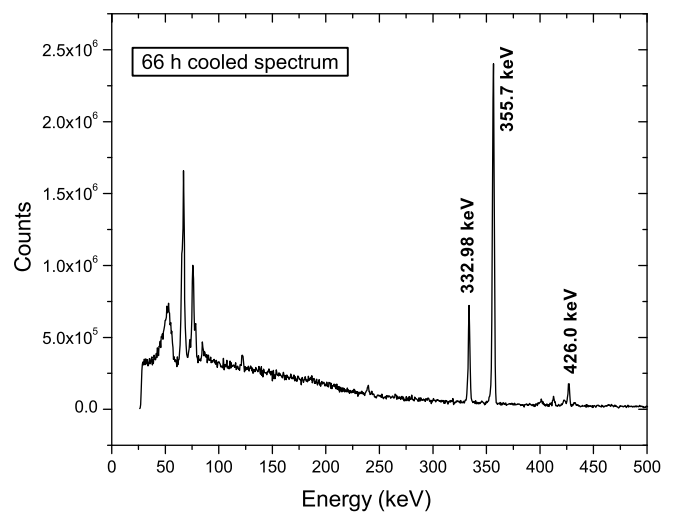


Fig. 2. Typical γ -ray spectrum of an irradiated gold foil showing the γ -lines of ^{196}Au .

software PHAST [15]. Typical γ -ray spectrum of irradiated and ^{197}Au and ^{197}Nb are given in Figs. 2 and 3 respectively.

3. Data analysis

3.1 Calculation of photon flux

The net peak area (A_{net}) corresponding to the photo-peak was calculated by summing the counts under the full energy peak and subtracting the linear Compton background. The photon flux was determined based on the activity of 355.7 keV γ -line of ^{196}Au from the $^{197}\text{Au}(\gamma, n)$ reaction [16, 17]. The photo-peak activities (A_{obs}) for 355.7 keV γ -line of ^{196}Au nuclide is related to the photon flux (ϕ) by the equation,

$$A_{\text{(net)}} \left(\frac{\text{CL}}{\text{LT}} \right) = \frac{N \langle \sigma \rangle \phi a \varepsilon (1 - e^{-\lambda t}) (e^{-\lambda T}) (1 - e^{-\lambda \text{CL}})}{\lambda} \quad (1)$$

Where, N is the number of target atoms, $\langle \sigma \rangle$ the average activation cross-section of the $^{197}\text{Au}(\gamma, n)^{196}\text{Au}$ reaction, ϕ

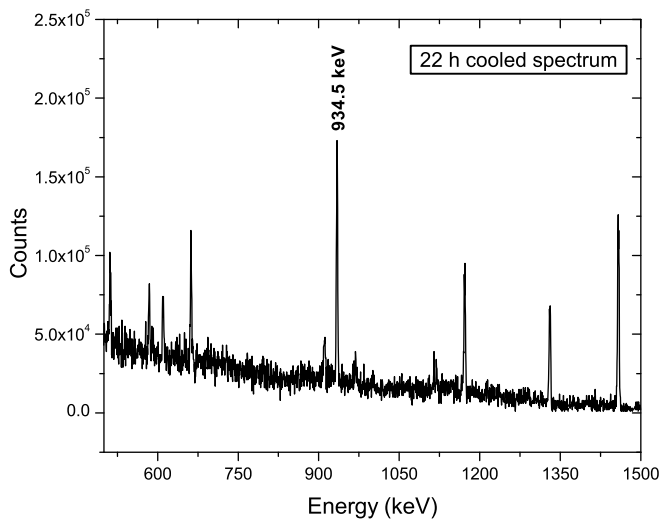


Fig. 3. Typical γ -ray spectrum of an irradiated ^{93}Nb showing the γ -line of $^{92\text{m}}\text{Nb}$.

is the bremsstrahlung flux, a the branching intensity of the analyzed γ -rays and ε the detection efficiency of the activated product. t , T , CL and LT are the irradiation time, cooling time, clock time and time duration for counting, respectively. λ is the decay constant for the isotope.

In the above equation the peak area has been corrected for dead time by multiplying by CL/LT factor.

The γ -ray energies and the decay data for the residual nuclide such as branching ratio, half-lives are taken from refs [18, 19] and are given in Table 1.

The average cross-section $\langle\sigma\rangle$ for $^{197}\text{Au}(\gamma, n)^{196}\text{Au}$ reaction was calculated using the following relation.

$$\langle\sigma\rangle = \frac{\sum \sigma\varphi}{\sum \varphi} \quad (2)$$

The photon flux distribution for bremsstrahlung end point energies of 10 and 12.5 MeV were calculated by using the EGS4 code [20]. The photon flux (φ) distribution with respect to photon energy (E) is presented in Fig. 4. Photo nuclear cross-sections (σ) of $^{197}\text{Au}(\gamma, n)^{196}\text{Au}$ reaction have been reported by many groups [21–24]. For our calculation, we have used the σ value from ref [25] for mono-energetic photons, which is shown in Fig. 5. For a particular energy E , the $\langle\sigma\rangle$ was obtained from literature data [25] of mono-energetic photons as well as from the theoretical value based on the TALYS 1.4 [14] computer code (Fig. 5). The flux-weighted average σ values for the $^{197}\text{Au}(\gamma, n)^{196}\text{Au}$ reaction from the literature and theoretical data are shown in Table 2. Then, the photon flux for the $^{197}\text{Au}(\gamma, n)^{196}\text{Au}$ reaction was calculated using the Eq. (1) by rearranging the terms.

Table 1. Nuclear spectroscopic data of the radio-nuclides from the $^{197}\text{Au}(\gamma, n)$ and $^{93}\text{Nb}(\gamma, n)$ reactions.

Nuclide	Half-life	γ -ray energy (keV)	γ -ray abundance (%)	Reactions	Q -value (MeV)	Threshold (MeV)
^{196}Au	6.183 d	332.983	22.9	$^{197}\text{Au}(\gamma, n)$	−8.0723	8.0725
		355.689	87			
		426.0	7			
$^{92\text{m}}\text{Nb}$	10.15 d	934.46	99	$^{93}\text{Nb}(\gamma, n)$	−8.8312	8.8317

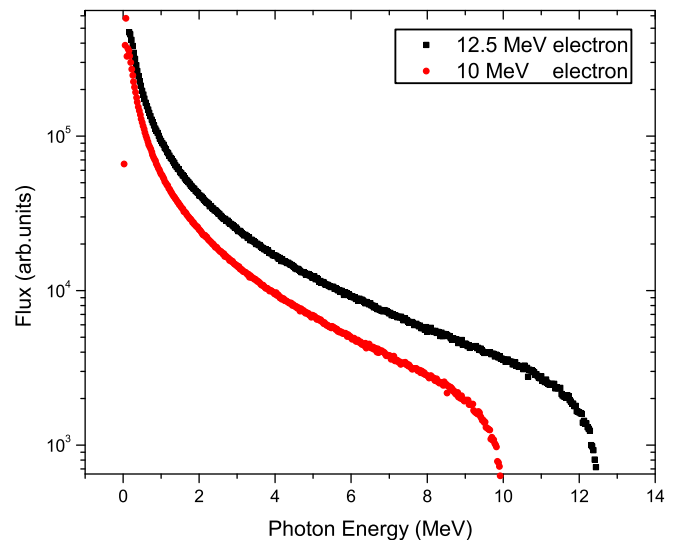


Fig. 4. Plot of bremsstrahlung spectrum for end point energies of 10 and 12.5 MeV.

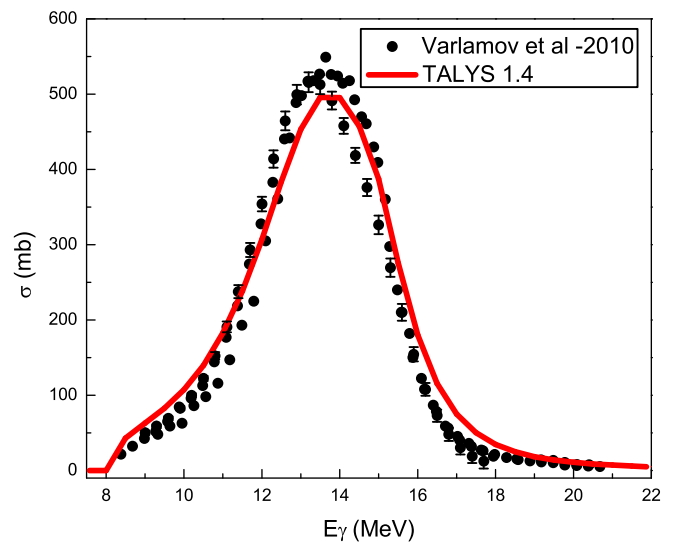


Fig. 5. Plot of experimental and theoretical $^{197}\text{Au}(\gamma, n)^{196}\text{Au}$ reaction cross-sections as a function of photon energy.

The threshold for the $^{197}\text{Au}(\gamma, n)^{196}\text{Au}$ and $^{93}\text{Nb}(\gamma, n)^{92\text{m}}\text{Nb}$ reactions are 8.073 MeV and 8.832 MeV, respectively. Thus the photon flux obtained from the $^{197}\text{Au}(\gamma, n)^{196}\text{Au}$ reaction has to be modified for the $^{93}\text{Nb}(\gamma, n)^{92\text{m}}\text{Nb}$ reaction based on threshold value to bremsstrahlung end point energy. In case of bremsstrahlung end point energy of 10 MeV, the weighted average flux obtained from the $^{197}\text{Au}(\gamma, n)^{196}\text{Au}$ reaction is multiplied by 0.4825, which is

Table 2. Measured cross-section of the $^{93}\text{Nb}(\gamma, n)^{92}\text{Nb}$ reaction at bremsstrahlung end point energies of 10 and 12.5 MeV.

Nuclide	Photon energy (MeV)	Flux-weighted $^{197}\text{Au}(\gamma, n)$ $\langle\sigma\rangle$ (mb) [Ref]	Flux (φ) $\times 10^8$ (Photons/cm ² /s)	γ -ray energy (keV)	σ (mb)
^{92}Nb	10	38.65 [25]	13.649 ± 0.22	934.46	4.923 ± 0.120
^{92}Nb	12.5	95.35 [25]	4.159 ± 0.037	934.46	9.137 ± 0.079
^{92}Nb	10	55 [14]	9.592 ± 0.155	934.46	6.993 ± 0.171
^{92}Nb	12.5	113.859 [14]	3.483 ± 0.031	934.46	10.900 ± 0.048

the flux ratio of $^{93}\text{Nb}(\gamma, n)^{92}\text{Nb}$ reaction from 8.825 MeV to 10 MeV to the $^{197}\text{Au}(\gamma, n)^{196}\text{Au}$ reaction from 8.07 MeV to 10 MeV. In case of bremsstrahlung end point energy of 12.5 MeV, the weighted average flux obtained from the $^{197}\text{Au}(\gamma, n)^{196}\text{Au}$ reaction is multiplied by 0.747, which is the flux ratio of $^{93}\text{Nb}(\gamma, n)^{92}\text{Nb}$ reaction from 8.825 MeV to 12.5 MeV to the $^{197}\text{Au}(\gamma, n)^{196}\text{Au}$ reaction from 8.07 MeV to 12.5 MeV. Experimentally obtained photon fluxes are summarized in Table 2.

3.2 Calculation of $^{93}\text{Nb}(\gamma, n)^{92}\text{Nb}$ reaction cross-sections

The radio-nuclide ^{92}Nb is produced from the $^{93}\text{Nb}(\gamma, n)^{92}\text{Nb}$ reaction. The niobium nucleus can be left in either its ground state ^{92}Nb or in its first excited state $^{92\text{m}}\text{Nb}$ which decays through the emission of a characteristic γ -line of 934.4 keV with absolute intensity of 99%. It is impossible to measure the decaying gamma's from the ground state of ^{92}Nb because of the quite long half-life of 3.5×10^7 yr. In the present work, we considered the gamma decays only from the excited state of $^{92\text{m}}\text{Nb}$ having a half life of 10.15 days. Since ^{92}Nb having m - and g -states, 55.2% of the total cross-section of $^{93}\text{Nb}(\gamma, n)^{92}\text{Nb}$ reaction contributed to the excited state of $^{92\text{m}}\text{Nb}$ [13].

The photo-neutron cross-section (σ) of ^{93}Nb was calculated from the net photo-peak area (A_{net}) of $^{92\text{m}}\text{Nb}$ using the equation

$$\sigma = \frac{A_{\text{net}} \left(\frac{\text{CL}}{\text{LT}} \right) \lambda}{N \varphi \varepsilon (1 - e^{-\lambda t}) (e^{-\lambda T}) (1 - e^{-\lambda \text{CL}})} \quad (3)$$

All the terms have the similar meaning as in the Eq. (1). The decay data of the radioactive products contributing $^{93}\text{Nb}(\gamma, n)^{92\text{m}}\text{Nb}$ reaction process and threshold energies are taken from the references [18, 26] and are presented in Table 1.

4. Results and discussion

The $^{93}\text{Nb}(\gamma, n)^{92\text{m}}\text{Nb}$ reaction cross-section determined in the present work at bremsstrahlung end point energies of 10 and 12.5 MeV are given in Table 2. In Table 2, the $^{93}\text{Nb}(\gamma, n)^{92\text{m}}\text{Nb}$ reactions cross-sections are based on the bremsstrahlung flux obtained from flux-weighted $^{197}\text{Au}(\gamma, n)^{196}\text{Au}$ reaction cross-section data of mono-energetic photon from Ref. [25]. On the other hand, the $^{93}\text{Nb}(\gamma, n)^{92\text{m}}\text{Nb}$ reactions cross-sections are based on the bremsstrahlung flux obtained from flux-weighted $^{197}\text{Au}(\gamma, n)$

^{196}Au reaction cross-section data of mono-energetic photon from TALYS 1.4 [14].

The uncertainties associated to the measured cross-sections come from the combination of two experimental data sets. This overall uncertainty is the quadratic sum of both statistical and systematic errors. The random error in the observed activity is primarily due to counting statistics, which is estimated to be 5–10%. This can be determined by accumulating the data for an optimum time period that depends on the half-life of the nuclides of interest. The systematic errors are due to uncertainties in photon flux estimation ($\sim 2\%$), the irradiation time ($\sim 0.5\%$), the detection efficiency calibration ($\sim 3\%$), the half-life of the reaction products and the γ -ray abundances ($\sim 2\%$). Thus the total systematic error is about $\sim 4.15\%$. The overall uncertainty is found to range between 6.5 and 10.8%, coming from the combination of a statistical error of 5–10% and a systematic error of 4.15%.

Results of the present photo-nuclear cross-sections of $^{93}\text{Nb}(\gamma, n)^{92\text{m}}\text{Nb}$ reactions at bremsstrahlung end point energies of 10 and 12.5 MeV were determined for the first time. In literature [12], there is only one set of data available for $^{93}\text{Nb}(\gamma, n)^{92}\text{Nb}$ reaction cross-section based on mono-energetic photons using the neutron counting method by the Saclay group. Their calculation was based on the total $^{93}\text{Nb}(\gamma, n)^{92}\text{Nb}$ reaction cross-section, which is shown in Fig. 6. The $^{93}\text{Nb}(\gamma, n)^{92}\text{Nb}$ reaction cross-section are available in Ref. [13] for bremsstrahlung energies above 26 MeV but not at the lower energy side. However, in the present measurement the data obtained is on the lower energy side and is based on off-line gamma ray counting method.

It can be seen from Fig. 6 that the $^{93}\text{Nb}(\gamma, n)^{92}\text{Nb}$ reaction cross-section increases with photon energy up to 14–16 MeV and thereafter decreases up to 20 MeV. The higher cross-section value for $^{93}\text{Nb}(\gamma, n)^{92}\text{Nb}$ reaction at end point bremsstrahlung energy of 12.5 MeV in the present work is due to the GDR effect. In order to examine this, the $^{93}\text{Nb}(\gamma, n)^{92}\text{Nb}$ reaction cross-section corresponding to the meta stable state and the total cross section as a function of photon energy was also calculated theoretically using the TALYS code 1.4 [14].

TALYS is a computer code basically used for analysis of basic scientific experiments or to generate nuclear data for applications. The basic objective behind its construction is the simulation of nuclear reactions that involve neutrons, photons, protons, deuterons, tritons, ^3He - and alpha-particles, in the 1 keV to 200 MeV energy range and for target nuclides of mass 12 and heavier. In TALYS, cross-sections for reac-

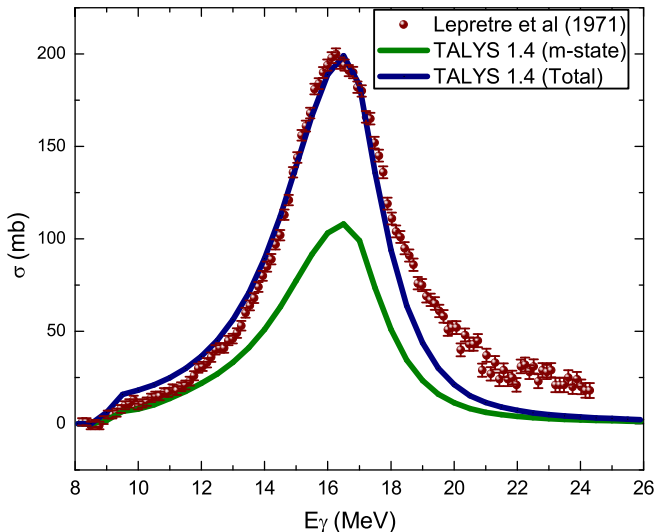


Fig. 6. Plot of experimental $^{93}\text{Nb}(\gamma, n)^{92}\text{Nb}$ reaction cross-sections (total) and theoretical $^{93}\text{Nb}(\gamma, n)^{92}\text{Nb}$ reaction cross-section (m-state and total) as a function of photon energy.

tions to all open channels are calculated. Several options are included for the choice of different parameters such as γ -strength functions, nuclear level densities and nuclear model parameters *etc.* In the present work, we calculated photon-induced reaction cross-section on a ^{93}Nb target using the default option in the TALYS code [14]. All possible outgoing channels possible for the given photon energy were considered. However, the cross-section for the (γ, n) reaction was specially looked for and collected. The (γ, n) reaction cross-section as a function of photon energy for and ^{93}Nb are also plotted in Fig. 6.

It can be seen from Fig. 6 that, the $^{93}\text{Nb}(\gamma, n)^{92}\text{Nb}$ reaction cross-section (total and the metastable state) as a function of photon energy from TALYS 1.4 shows a similar structure within the available experimental data [12]. However, the magnitude of theoretical $^{93}\text{Nb}(\gamma, n)^{92m}\text{Nb}$ reaction cross-section from TALYS is nearly half of the experimental data [12] at peak position. On the other hand, the total cross-section for $^{93}\text{Nb}(\gamma, n)^{92}\text{Nb}$ reaction is well reproduced by the TALYS 1.4. It can also be seen from the Fig. 6 that, in the total $^{93}\text{Nb}(\gamma, n)^{92}\text{Nb}$ reaction cross section using TALYS 1.4, a left side shift was observed from the threshold to 15 MeV and slight right side shift was observed from 15 MeV to 16.5 MeV as compared to the available literature data [12]. Then after it follows the path of available literature data up to 18 MeV and again a left side shift was observed. The theoretical $^{93}\text{Nb}(\gamma, n)^{92}\text{Nb}$ reaction cross-section from TALYS also clearly shows the GDR effect.

The flux weighted average cross-section for $^{93}\text{Nb}(\gamma, n)^{92}\text{Nb}$ reaction was obtained from the literature data [12], using Eq. (2) and given in Table 2. The flux weighted average cross-section for $^{93}\text{Nb}(\gamma, n)^{92}\text{Nb}$ reaction (total and metastable state) from theoretical value of TALYS 1.4 is also calculated and given in Table 2. It can be seen from the Table 2 that, the experimentally obtained $^{93}\text{Nb}(\gamma, n)^{92}\text{Nb}$ reaction cross-section based on 934.4 keV γ -line varies from 4.9–7.0 mb for end point bremsstrahlung energy of 10 MeV to 9.1–10.9 mb for 12.5 MeV. The variation in $^{93}\text{Nb}(\gamma, n)^{92}\text{Nb}$ reaction cross-section is due to the use of different types of photon flux based on experimen-

Table 3. Comparison of flux-weighted average $^{93}\text{Nb}(\gamma, n)$ reaction cross-sections based on experimental mono-energetic photons from literature [12] and TALYS 1.4 [14] with the experimental data of present work at bremsstrahlung end point energies of 10 and 12.5 MeV.

Photon energy (MeV)	Experimental <i>m</i> -state	Cross-section (mb)		
		(Total)	Literature (TALYS 1.4) (Total)	(Total)
10	4.923	9.846	7.159	11.263
12.5	9.137	18.274	13.965	17.324

tal and theoretical $^{197}\text{Au}(\gamma, n)^{196}\text{Au}$ reaction cross-section, which are shown in Table 2.

The experimentally determined $^{93}\text{Nb}(\gamma, n)^{92m}\text{Nb}$ reaction cross-section at bremsstrahlung end point energies of 10 and 12.5 MeV along with the flux-weighted value from literature [12] and TALYS 1.4 [14] are given in Table 3 for comparison. It can be seen from Table 3 that the experimentally determined $^{93}\text{Nb}(\gamma, n)^{92m}\text{Nb}$ reaction cross-section at bremsstrahlung end point energies of 10 and 12.5 MeV are closer to the flux weighted value obtained from TALYS 1.4 [14]. However, the experimentally determined $^{93}\text{Nb}(\gamma, n)^{92m}\text{Nb}$ reaction cross-section at both energies are lower than the flux weighted value obtained from literature data [12] since the available experimental $^{93}\text{Nb}(\gamma, n)^{92}\text{Nb}$ reaction cross section measured using neutron counting method is the total reaction cross-section. For the total $^{93}\text{Nb}(\gamma, n)^{92}\text{Nb}$ reaction cross-section, the flux weighted values obtained from TALYS 1.4 is higher compare to the flux weighted values from literature data. The higher cross-section value for $^{93}\text{Nb}(\gamma, n)^{92}\text{Nb}$ reaction at bremsstrahlung end point energy of 12.5 MeV compared to that of 10 MeV may be due to the GDR effect.

5. Conclusions

The cross section of the $^{93}\text{Nb}(\gamma, n)^{92}\text{Nb}$ reaction at bremsstrahlung end point energies of 10 and 12.5 MeV has been measured using activation technique. High resolution γ -ray spectrometry was used to determine the photo neutron cross section of ^{93}Nb . The $^{93}\text{Nb}(\gamma, n)^{92m}\text{Nb}$ reaction cross-sections increases from 10 to 12.5 MeV, which indicates the role of excitation energy. Theoretically, the $^{93}\text{Nb}(\gamma, n)^{92}\text{Nb}$ reaction cross-section as a function of photon energy was also calculated using the TALYS 1.4 code. The flux-weighted average cross-section for $^{93}\text{Nb}(\gamma, n)^{92}\text{Nb}$ reactions at bremsstrahlung end point energies of 10 and 12.5 MeV have been obtained from the values of TALYS and literature data based on mono-energetic photon. The experimentally determined $^{93}\text{Nb}(\gamma, n)$ reaction cross-section at bremsstrahlung end point energies of 10 and 12.5 MeV are closer to the flux weighted value of TALYS. The higher cross-section of $^{93}\text{Nb}(\gamma, n)^{92}\text{Nb}$ reaction at bremsstrahlung end point energy of 12.5 MeV compared to that of 10 MeV may be due to the GDR effect.

Acknowledgment. The authors are thankful to the staff of electron LINAC at EBC, Kharghar, Navi-Mumbai and Dr. L. M. Gantayet, Group Director of the BTD group, BARC for providing the electron beam to carry out the experiments. Financial support from the Re-

search in Nuclear sciences (BRNS), DAE, Government of India, is gratefully acknowledged by one of the authors Mrs. Rita Crasta. The authors wish to thank fellow researchers and technical staffs at the Microtron Centre, Mangalore University for their help.

References

1. IAEA-TECDOC-1178: Handbook on Photonuclear Data for Applications Cross-Sections and Spectra, available online at: <http://www-nds.iaea.org>.
2. Chadwick, M. B., Hughes, H. G., Little, R. C., Pitcher, E. J., Young, P. G.: *Progress Nucl. Energ.* **38**, 179 (2001).
3. Ganesan, S.: *Pramana, J. Phys.* **68**, 257 (2007).
4. Maitreyee Nandy, Sarkar, P. K., Nakao, N., Shibata, T.: *PRA-MANA J. Phys.* **73**, 669 (2009).
5. Murty, K. L., *Appl. Mech. Rev.* **46** (5), 194 (1993).
6. Choo, K. N., Kang, Y. H., Pyun, S. I., Urbanic, V. F.: *J. Nucl. Mater.* **209**, 226 (1994).
7. Sabol, G., Klip, G. R., Balfour, M. G., Roberts, E.: *Zirconium in Nuclear Industry*. In: 8th International Symposium (ASTM STP), Philadelphia (1989), vol. 1023, p. 227.
8. Sabol, G. P., Schoenberger, G., Balfour, M. G. IAEA Tech. Comm. Meeting on Materials for Advanced Water-Cooled Reactors. Plzen, Czech and Slovak Federal Republic, IAEA (1991), p. 50.
9. Chowdhury, P. S., Mukherjee, P., Gayathri, N., Bhattacharya, M., Chatterjee, A., Barat, P., Nambissan, P. M. G.: *Bull. Mater. Sci.* **34**, 507 (2011).
10. Bowman, C. D.: *Annu. Rev. Nucl. Part. Sci.* **48**, 505 (1998).
11. Adam, J., Balabekyan, A. R., Barashenkov, V. S., Brandt, R., Golovatiouk, V. M., Kalinnikov, V. G., Katovsky, K., Krivopustov, M. I., Kumar, V., Kumawat, H., Odoj, R., Pronskikh, V. S., Solnyshkin, A. A., Stegailov, V. I., Tsoupko-Sitnikov, V. M., Westmeier, W.: *Eur. Phys. J. A* **23**, 61 (2005).
12. Lepretre, A., Beil, H., Bergere, R., Carlos, P., Veyssiere, A.: *Nucl. Phys. A* **175**, 609 (1971).
13. Rahman, A. K. Md. L., Kato, K., Arima, H., Shigyo, N., Ishibashi, K., Hori, J., Nakajima, K.: *J. Nucl. Sci. Tech.* **47**, 618 (2010).
14. Koning, A. J., Hilaire, S., Duijvestijn, M. C.: *Proceedings of the International Conference On Nuclear Data for Science and Technology, ND 2004, Santa Fe, 2004* (Haight, R. C., Chadwick, M. B., Kawano, T., Talou, P., eds.), AIP Conf. Proc. (2005), vol. 769, p. 1154.
15. Mukhopadhyay, P. K.: *Proceedings of the Symposium on Intelligent Nuclear Instrumentation (INIT-2001)*, Bhabha Atomic Research Centre, Mumbai (2001), p. 307.
16. Yoshinaga, O., Toyooki, K., Nobuyoshi, S.: *Bull. Chem. Soc. Japan* **42**, 387 (1969).
17. Yamadera, A., Yoshitomo, U., Nakamura, T.: *Nucl. Instrum. Methods Phys. Res. A* **329**, 188 (1993).
18. Browne, E., Firestone, R. B.: *Table of Radioactive Isotopes*. (Shirley, V. S., ed.) John Wiley & Sons, New York (1986); Firestone, R. B., Ekstrom, L. P.: *Table of Radioactive Isotopes*. Version 2.1, Lawrence Berkeley National Laboratory, Berkeley (2004), <http://ie.lbl.gov/toi/index.asp>.
19. Xiaolong, H.: *Nucl. Data Sheets* **108**, 1093 (2007).
20. Nelson, W. R., Hirayama, H., Rogers, D. W. O.: SLAC report 265 (1985).
21. Veyssiere, Beil, H., Bergere, R., Carlos, P., Lepretre, A.: *Nucl. Phys. A* **159**, 561 (1970).
22. Fultz, C., Bramblett, R. L., Caldwell, J. T., Kerr, N. A.: *Phys. Rev.* **127**, 1273 (1962).
23. Vogt, K., Mohr, P., Babilon, M., Bayer, W., Galaviz, D., Hartmann, T., Hutter, C., Rauscher, T., Sonnabend, K., Volz, S., Zilges, A.: *Nucl. Phys. A* **707**, 241 (2002).
24. Hara, K. Y., Harada, H., Kitatani, F., Goko, S., Hohara, S. Ya., Kaihori, T., Makinaga, A., Utsunomiya, H., Toyokawa, H., Yamada, K.: *J. Nucl. Sci. Tech.* **44**, 938 (2007).
25. Varlamov, V. V., Ishkhanov, B. S., Orlin, V. N., Troshchiev, S. Yu.: *Izv. Ross. Akad. Nauk, Ser. Fiz.* **74**, 884 (2010).
26. Kocher, D. C., Horen, D. J.: *Nucl. Data Sheets B* **7**, 299 (1972).